

DOI: 10.1093/jcde/gwaf032

Advance access publication date: 18 March 2025 Research Article

# Finite element and long short-term memory analysis for impact of nanoparticle shape on hybrid nanofluid flow in a lid-driven cavity

Umair Rashid¹, Ashmore Mawire², Qingyuan Wang¹,³, Ali J. Chamkha⁴ and Kun Yang¹,³,\*

- <sup>1</sup>Institute for Advanced Study, Chengdu University, Chengdu 610106, P.R. China
- $^2$ Material Science, Innovation and Modelling (MaSIM), North-West University, Mmabatho 2745, South Africa
- <sup>3</sup>Failure Mechanics and Engineering Disaster Prevention and Mitigation Key Laboratory of Sichuan Province, Sichuan University, Chengdu 610065, China
- $^4$ Faculty of Engineering, Kuwait College of Science and Technology, Doha District, 35004, Kuwait

#### **Abstract**

The significance of nanoparticle shapes is evident in various domains of detecting trace metals in biomolecular assays and nanotechnology applications. The present study focused on copper and aluminum-water hybrid nanofluid flow inside a lid-driven cavity. The heated elliptic-shaped obstacle is emended inside the lid-driven square cavity. The hybrid nanofluid contained water and two categories of nanoparticles with sphere, column, and lamina shapes. The solution of the projected model governing equations is evaluated by the Galerkin Method. Long short-term memory is used to ensure the accuracy of the solution and comparison of results. The characteristics of hybrid nanofluid are presented as streamlines, isothermal contour plots, kinetic energy, and heat transfer. The graphical description shows that lamina-shaped nano-sized particles dominate the distribution of temperature and heat transfer. The long short-term memory approach demonstrated high accuracy in our comparative analysis.

Keywords: nanoparticle shape, hybrid nanofluid, finite element method, long short-term memory

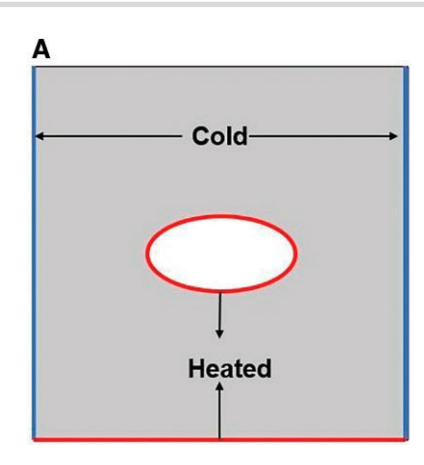
#### 1. Introduction

Numerous vital applications can be achieved by using nanoparticle shapes and sizes. The significance of nanoparticle shapes is evident in various domains of detecting trace metals in biomolecular assays and nanotechnology applications (Knauer & Koehler, 2016). It is accepted in the field of fluid dynamics the shape of nanoparticles plays a crucial role in the transportation dynamics within confined channels, especially in narrow tubes (Caldorera-Moore et al., 2010). Sphere-shaped nanoparticles are extensively studied in biomedical fields involving biosensing and bioimaging, theranostics, and diagnostics, but the effect of nanoparticles shape has received little consideration (Zhao et al., 2017). Spherical-shaped nanoparticles have been noted to be the main factor accumulating in different organs responsible for clearance, such as the spleen, kidney, and liver (Truong et al, 2017). The unique characteristics of non-spherical shaped nanoparticles recommend that intelligent control over nanoparticle geometry can move the paradigm in nanomedicine from spherical nanoparticles to those with further complex geometries. The intersection of nanoparticles with cells in the blood vessels and bloodstream, subsequent cellular binding, intercellular transport, uptake, transport across the endothelial wall into the tumor, and clearance rate of unbounded nanoparticles are dependent on the geometry of nanoparticles. For example, a non-spherical nanoparticle design can show increased targeted drug delivery efficiency and circulation time in living subjects.

They can also explore, migrate, and bind to tumor vasculature more efficiently (Zhu et al., 2019).

Nowadays, the latest method applied for heat transfer in fluids is identified as a hybrid nanofluid (Rashid et al., 2023a). Hybrid nanofluids have piqued the interest of scientists, engineers, and scholars due to their comprehensive applications in various fields, including microfluidics, medical lubrication, transportation, and manufacturing. Their adaptability extends to areas such as solar heating, generator cooling, acoustics, and maritime structures, making them indispensable in technical and industrial domains (Jamil & Ali, 2020). This remarkable versatility arises from their unique composition, where two dissimilar nano-sized particles with different physical and chemical properties are combined with a base fluid, creating a hybrid nanofluid with enhanced thermal and flow characteristics (Qureshi et al., 2023). Tanzila and Nadeem (Aziz et al., 2018) deliberated the heat transfer in water-(Ag/CuO) and water/CuO hybrid nanofluids over a rotating surface with the impact of heat generation, chemical reaction, and radiation. Sakkaravarthi et al. (2024) discussed the heat transfer in Casson tetra hybrid nanofluid flow using the Levenberg Marquardt neural network approach. Al-mdallal et al. (2020) examined the impacts of Marangoni radiative convection in (Al<sub>2</sub>O<sub>3</sub>/SiO<sub>2</sub>)-H<sub>2</sub>O, (Al<sub>2</sub>O<sub>3</sub>/TiO<sub>2</sub>)-water, and (TiO<sub>2</sub>/SiO<sub>2</sub>)-water hybrid nanofluid on flow and heat transfer past a permeable surface in the existence of the magnetic field. Najiyah Safwa Khashi'ie et al. (2020) examined the thermal Marangoni flow and energy transfer of water-(Al<sub>2</sub>O<sub>3</sub>/Cu) hybrid nanofluid over a shrinking

<sup>\*</sup>Correspondence: scu\_yangkun@163.com



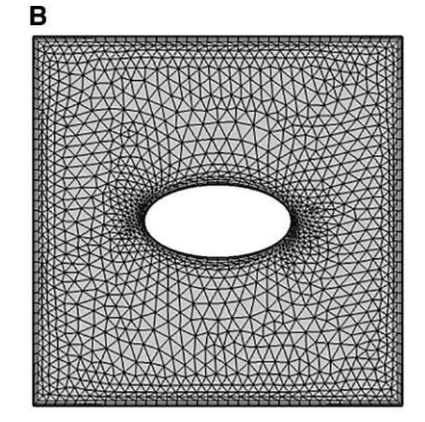


Figure 1: The geometry of the problem (A) and (B) mesh distribution.

**Table 1:** The numerical values of shape factors (Rashid & Ibrahim, 2020).

Shapes	Sphere	Column	Lamina
Phi	1	0.4710	0.1857
q	3	6.3698	16.1576

Table 2: Thermophysical properties of (Cu and Al<sub>2</sub>O<sub>3</sub>)/H<sub>2</sub>O (Bhuiyana et al., 2017).

Physical properties	Cu	$Al_2O_3$	H <sub>2</sub> O
k (W/m K)	401	40	0.613
$\rho$ (kg/m <sup>3</sup> )	9833	3970	997.1
$\beta \times 10^{-5} \text{ K}^{-1}$	1.67	0.85	21
C <sub>p</sub> (J/kg K)	385	765	4179

and stretching sheet. Afrand et al. (2016) scrutinized the nanoparticle's influence on temperature and concentration distribution in (Fe $_3$ O $_4$  and Ag)/ethylene glycol hybrid nanofluid flow. Waini et al. (2020) numerically discussed the solution of (Al $_2$ O $_3$ /Cu)-H $_2$ O hybrid nanofluid stagnation point flow and heat transfer past a shrinking and stretching cylinder. Khan et al. (2011) studied bioconvective and chemically reactive combined nanofluid flow on a horizontally moving needle. Ahmad et al. (2023) did experimental work to analyse the performance of heat transfer in  $(Al_2O_3$ and Zn)/water hybrid nanofluid. Akbar et al. (2024) discussed the (Al<sub>2</sub>O<sub>3</sub> and Cu)/water hybrid nanofluid flow and heat transfer over a stretching sheet by using artificial neural networks.

For many years, finite element method-based solutions of fluid dynamics have been expended in quality and quantity. The finite element method and finite volume method are both highly effective methods for solving problems related to computational fluid dynamics (Nithiarasu & Zienkiewicz, 2006). Fayz-Al-Asad et al. (2024) utilized the finite element method to examine the thermal enhancement in (Cu-water) nanofluid flow in an undulating wavy cavity. Srinivasa et al. (2016) applied the finite element method to examine the numerical solution of unsteady hydromagnetic natural convection Couette flow between two vertical parallel plates. Hughes et al. (1979) studied the incompressible viscous fluid flow by using the finite element method. Babazadeh et al. (2020) applied the finite element method (FEM) to investigate the hybrid nanofluid study within a permeable medium in the existence of Lorentz forces. Madhu and Kishan (2015) analysed the influences of magnetic field and thermal radiation in viscous incompressible and viscoelastic nanofluid flow past a stretching sheet by adopting the finite element method. Sohail et al. (2024) applied the finite element method to examine the effect of thermal radiation, time relaxation number, and magnetic field in cross-fluid flow over a vertical disc. Ibrahim and Lamesse (2023) used the finite element method to inspect the effect of Eyring Powell and magnetic parameters on nanofluid flow over a stretching sheet. Ali et al. (2024) applied the finite element method to examine the effect of material parameter, Hartmann number on micro-polar fluid flow induced by Riga plate.

Sepp Hochreiter and Jurgen Schmidhuber (Hochreiter, 1997; Chang et al., 2020) planned of a recurrent neural network (RNN) named long short-term memory (LSTM). This method is a unique deep learning network that is extensively applied for the prediction of time series data and text analysis, i.e., google developed into two layers of deep LSTM (Beaufays et al., 2014) to build largescale and speech recognition models. Deep learning is concerned with internal laws and external correlations linking input and output parameters that can be recognized by multi-hidden structures of deep learning algorithms (Zhang et al., 2018). The application of LSTM has gained popularity in the field of environmental science for example in the use of establishing effective and robust forecasting wind speed models and monitoring carbon dioxide fluxes in forest environments (Qian et al., 2019). Deep learning neural network prediction models like LSTM have revealed important advancements in many fields (Selvaggio et al., 2022). Qian et al. (2019) used LSTM for the prediction of toxic gas dispersion. They compared it with several network models, i.e., support vector machine, backpropagation, and Gaussian diffusion model. They noted that LSTM provided higher prediction accuracy.

An analysis of the referenced literature indicates that no attempts have been made to examine the comparative study of the impact of nanoparticle shape on hybrid nanofluid flow in a liddriven cavity. This current research represents a significant advancement in fluid dynamics, providing insights that can enhance the optimization and design of engineering systems for greater effectiveness and efficiency. In view of the above considerations, the present model is suitable for examining the numerical solution of the lid-driven cavity problem. These innovative techniques shed new light on applications in nanotechnology and hybrid fluids. Comparing the hybrid nanofluid flow using the Galerkin Method and LSTM is also a prominent aspect of this research work. The quality of nanofluid depends on the shape of the nanoparticles. Also, the originality of this work is to examine the performance

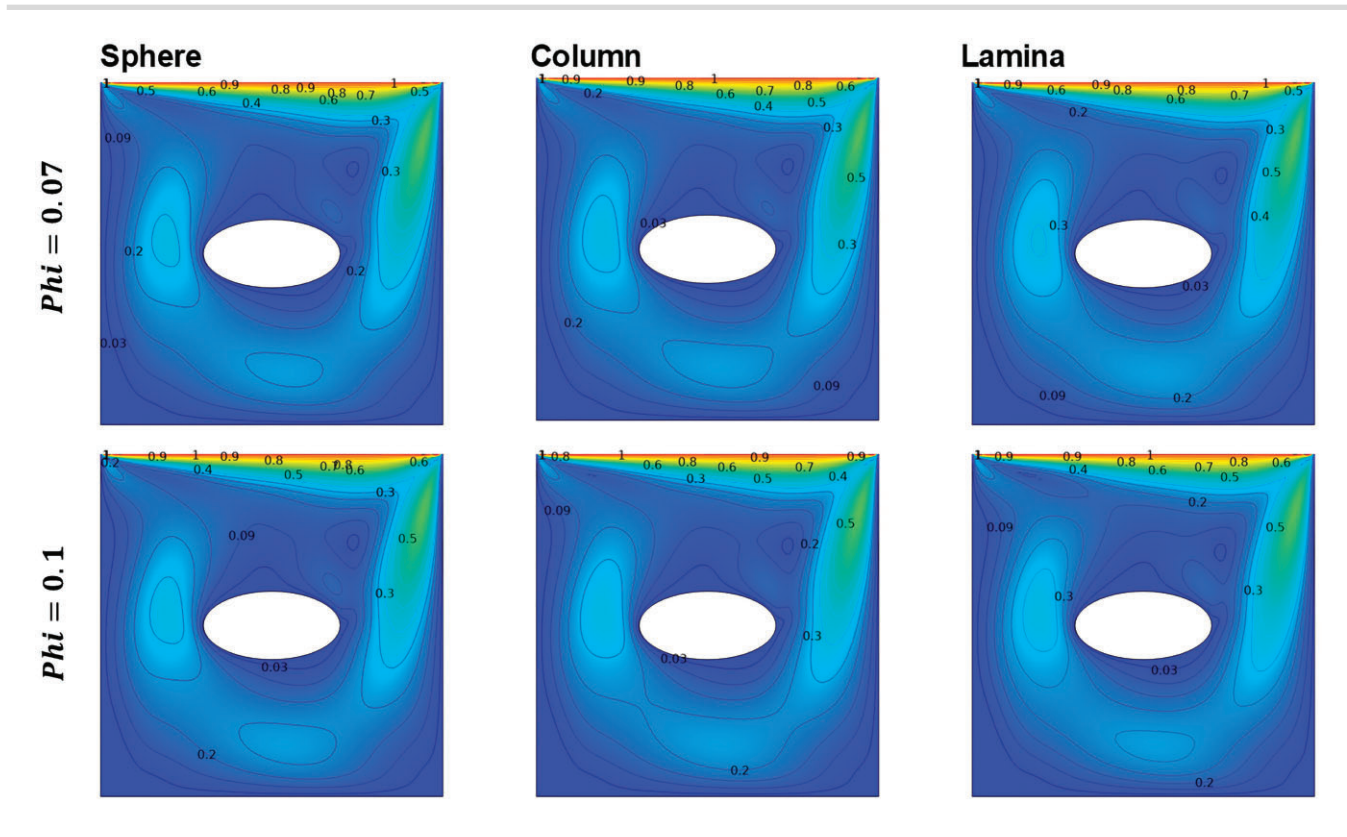


Figure 2: Impact of Phi on Streamlines for various nanoparticle shapes (Sphere, Column, Lamina).

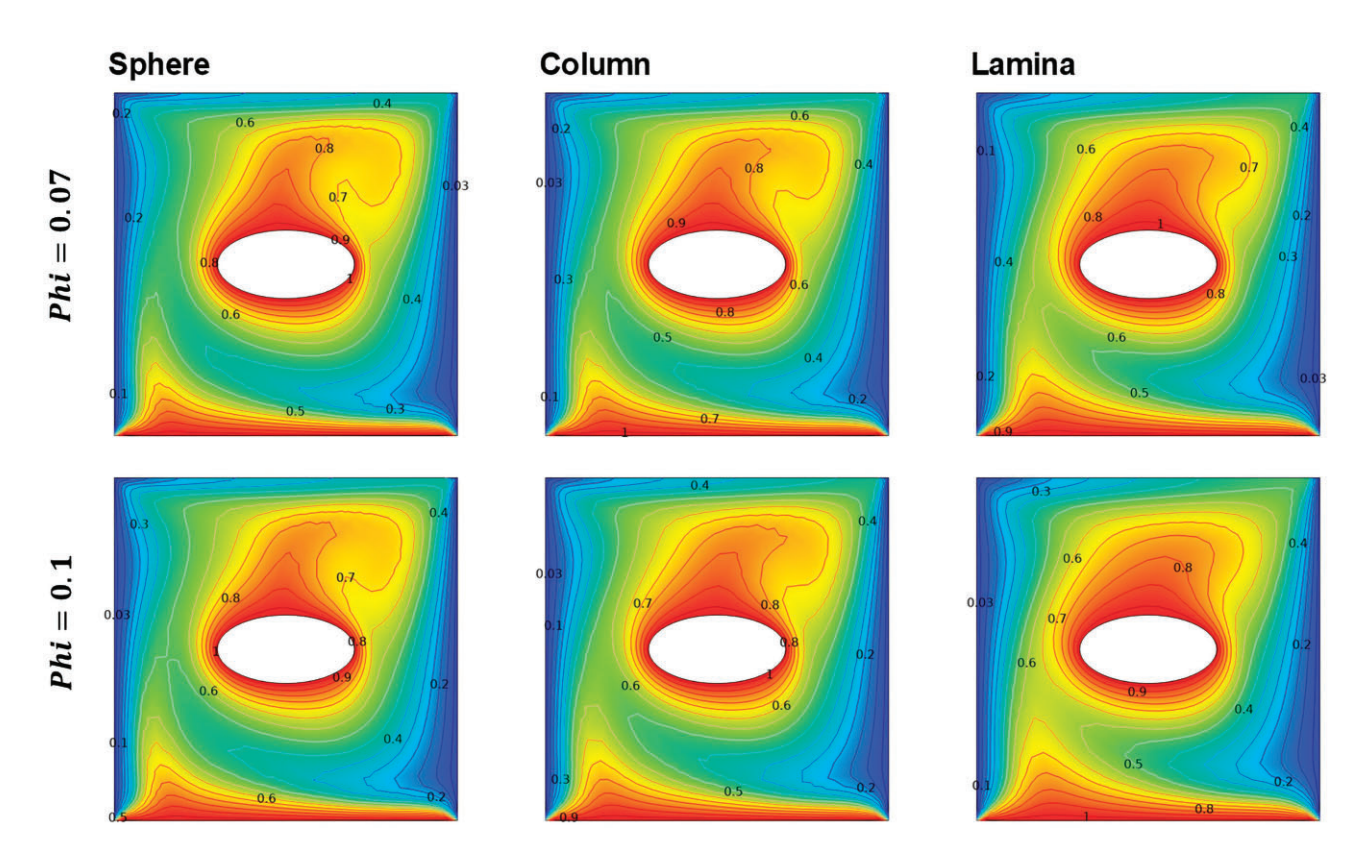


Figure 3: Impact of Phi on isotherms for various nanoparticle shapes (sphere, column, lamina).

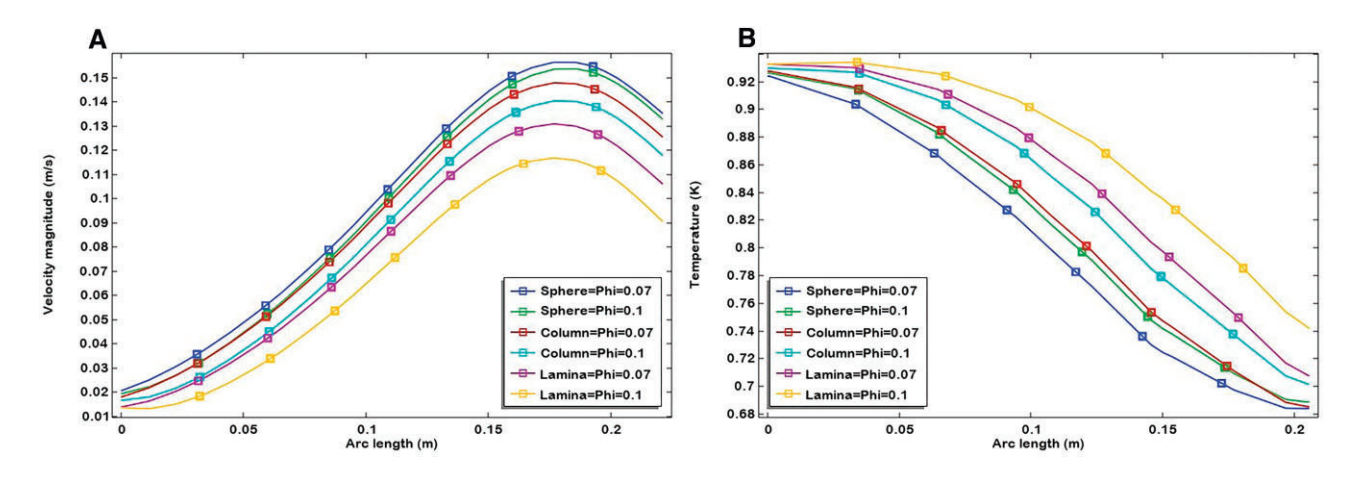


Figure 4: Influence of Phi: (A) on the velocity profile and (B) temperature distribution against different nanoparticle shapes (sphere, column, lamina).

Table 3: Impact of phi on K.E.

inetic energy
0.0 017 194
0.0016371
0.0016738
0.0 015 592
0.0 015 781
0.0014463

Table 4: Impact of phi on Nu.

Shape	Phi	Nusselt number
Sphere	0.05	0.53 529
-	0.1	0.67 051
Column	0.05	0.67 966
	0.1	0.95 906
Lamina	0.05	1.0515
	0.1	1.6973

of nanoparticle shapes in heat transfer of hybrid nanofluid with different techniques. High accuracy is demonstrated in comparisons of these methodologies. Tabular and graphical descriptions are considered to discuss the effects of physical parameters.

### 2. Physical Model

The physical configuration and domain discretization for the present study are shown in Figures 1A and B. It is assumed that a two-dimensional, steady hybrid nanofluid (copper and aluminawater) flow occurs inside a lid-driven square cavity with height H and length L, respectively. An elliptic-shaped heated obstacle is embedded within the cavity to regulate the flow and thermal distribution inside the domain. The left and right walls of the cavity are maintained at a cold temperature  $T_c$ , while the bottom wall and elliptic obstacle are heated to a temperature  $T_h$ . Additionally, the upper wall of the cavity is moving, adiabatic, and subject to a no-slip condition. The values of nanoparticle shape factors and thermophysical properties of (Cu and Al<sub>2</sub>O<sub>3</sub>)/H<sub>2</sub>O are explained in Table 1 and Table 2. The equations of the model are considered as (Rashid et al. 2023b).

$$\frac{\partial U}{\partial X} + \frac{\partial V}{\partial Y} = 0, \tag{1}$$

$$U\frac{\partial U}{\partial X} + V\frac{\partial U}{\partial Y} = -\frac{\partial P}{\partial X} + \frac{\nu_{hnf}}{\nu_f} \frac{1}{Re} \left( \frac{\partial^2 U}{\partial X^2} + \frac{\partial^2 U}{\partial Y^2} \right), \tag{2}$$

$$U\frac{\partial V}{\partial X} + V\frac{\partial V}{\partial Y} = -\frac{\partial P}{\partial Y} + \frac{\nu_{hnf}}{\nu_f} \frac{1}{Re} \left( \frac{\partial^2 V}{\partial X^2} + \frac{\partial^2 V}{\partial Y^2} \right) + \frac{(\rho \beta)_{hnf}}{(\rho \beta)_f} PrRi\theta, (3)$$

$$U\frac{\partial \theta}{\partial X} + V\frac{\partial \theta}{\partial Y} = \frac{\alpha_{hnf}}{\alpha_f} \frac{1}{PrRe} \left( \frac{\partial^2 \theta}{\partial X^2} + \frac{\partial^2 \theta}{\partial Y^2} \right), \tag{4}$$

To convert it into a nondimensional form following parameters

$$X = \frac{x}{L}, Y = \frac{y}{L}, U = \frac{u}{U_0}, V = \frac{v}{U_0}, P = \frac{P}{\rho_{vr} U_0^2}, Ri = \frac{Gr}{Re^2}, Re = \frac{U_0 L}{v_f},$$

$$Gr = \frac{g\beta_f(T_h - T_c)}{v_f^2}L^3, \ Pr = \frac{v_f}{\alpha_f}, \ \theta = \frac{T - T_c}{T_h - T_c},$$

$$\alpha_{hnf} = \frac{k_{kn_f}}{(\rho C p)_{nf}}, \alpha_f = \frac{k_f}{(\rho C p)_f}, \tag{5}$$

The dimensionless form of boundary values condition is

$$U=0, V=0, \theta=1$$
, at bottom wall and obstacle  $U=0, V=0, \theta=1$ , at left and right walls  $U=0, V=1$ ,  $\frac{\partial \theta}{\partial n}=0$ , at the top wall. (6)

$$\frac{\mu_{hn_f}}{\mu_f} = \frac{1}{(1-Phi1)^{2.5}} \cdot \frac{1}{(1-Phi2)^{2.5}},$$

$$\frac{
ho_{\mathrm{hn}_{\mathrm{f}}}}{
ho_{\mathrm{f}}} = (1 - \mathrm{Phi2}) (1 - \mathrm{Phi1}) \, 
ho_{\mathrm{f}} + 
ho_{\mathrm{s1}} \mathrm{Phi1} + 
ho_{\mathrm{s2}} \mathrm{Phi2},$$

$$(\rho Cp)_{hnf} = (1 - Phi2)(1 - Phi1)(\rho Cp)_f + (\rho Cp)_{s1}Phi1 + (\rho Cp)_{s2}Phi2,$$

$$\frac{k_{hn_f}}{kn_f} = \frac{\left[k_{s2} + (q-1)\,kn_f\right] - (q-1)\cdot Phi2\cdot \left(kn_f - k_{s2}\right)}{\left[k_{s2} + (q-1)\,kn_f\right] + Phi2\cdot \left(kn_f - k_{s2}\right)}$$

$$\frac{k_{n_f}}{k_f} = \frac{\left[k_{\text{S1}} + (q-1)\,k_f\right] - (q-1)\cdot\text{Phi1}\cdot\left(k_f - k_{\text{S1}}\right)}{\left[k_{\text{S1}} + (q-1)\,k_f\right] + \text{Phi1}\cdot\left(k_f - k_{\text{S1}}\right)},$$

$$(\rho\beta)_{nf} = (1 - Phi2)(1 - Phi1)(\rho\beta)_f + (\rho\beta)_{s1}Phi1 + (\rho\beta)_{s2}Phi2,$$
 (7)

The KE  $=\frac{1}{2}\int_{\Omega}||U||^2d\Omega$  [kinetic energy (KE)] and Nu  $=(-\frac{\partial\theta}{\partial X})_{X=0}$ (Nusselt number) are taken as

$$KE = \frac{1}{2} \int_{\Omega} ||U||^2 d\Omega, \tag{8}$$

$$Nu = \left(-\frac{\partial \theta}{\partial X}\right)_{X=0},\tag{9}$$

$$Nu_{avg} = \frac{k_{hn_f}}{kn_f} \int_0^1 NudY$$
 (10)

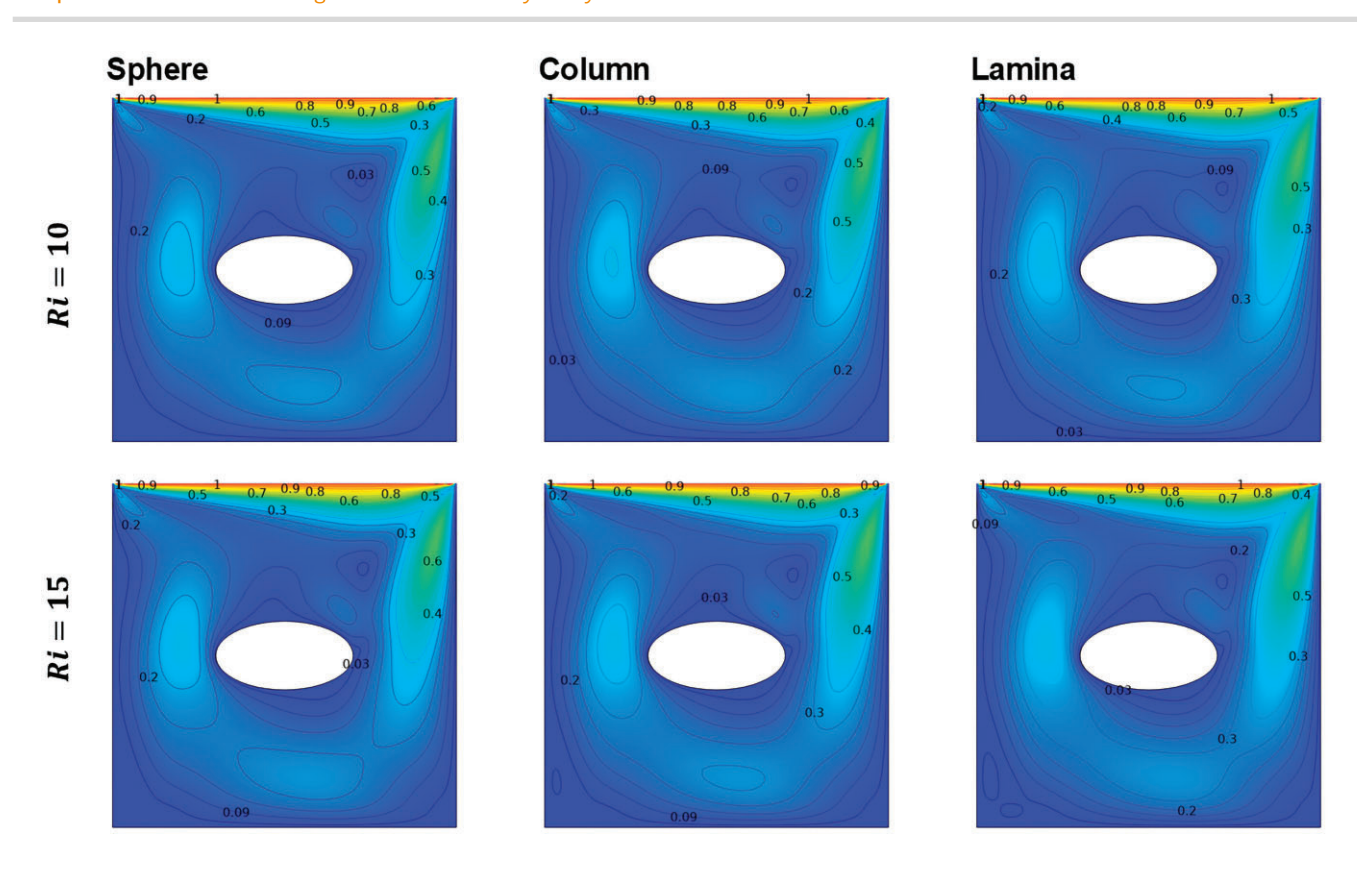


Figure 5: Impact of Ri on streamlines for different nanoparticle shapes (sphere, column, lamina).

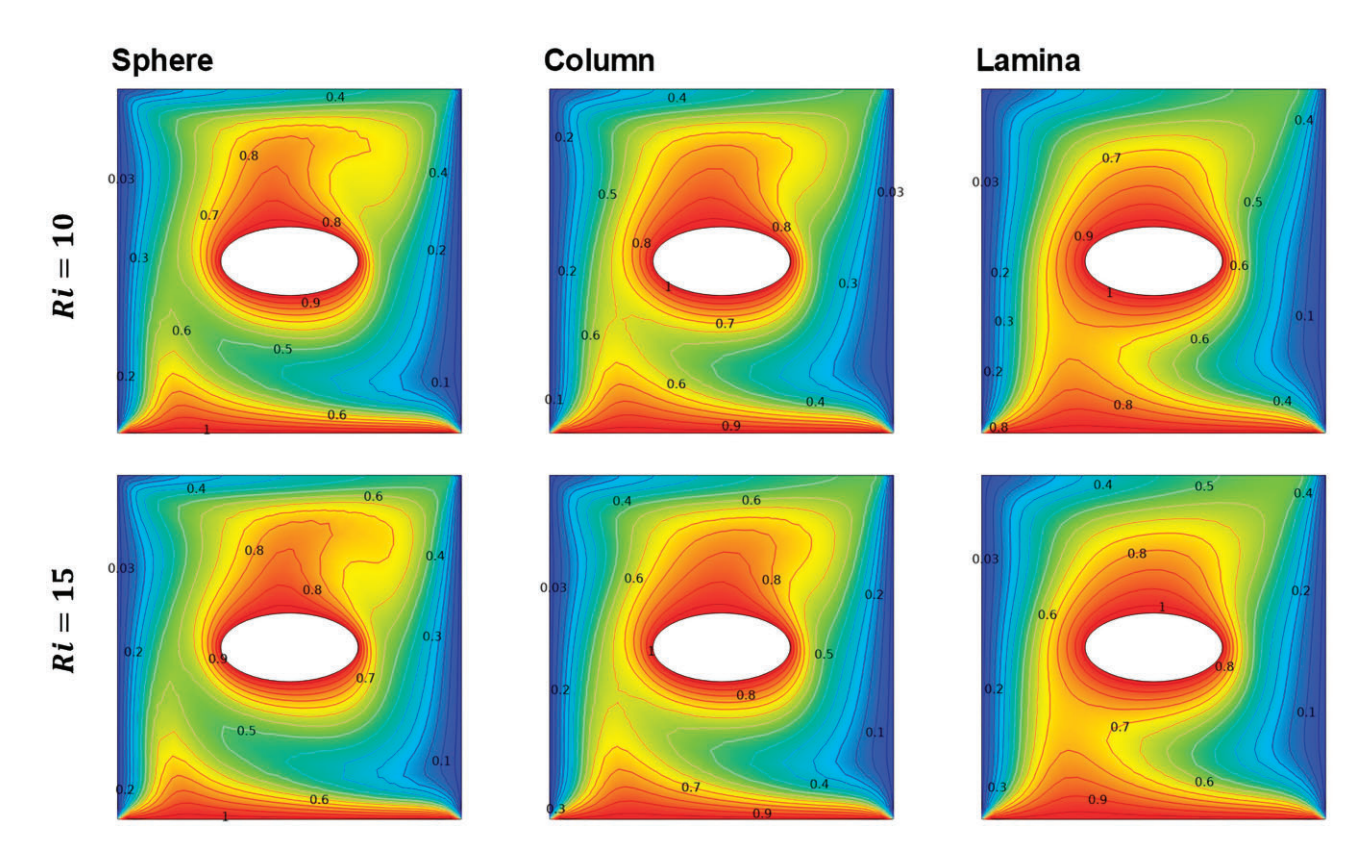


Figure 6: Impact of Ri on isotherms for different nanoparticle shapes (sphere, column, lamina).

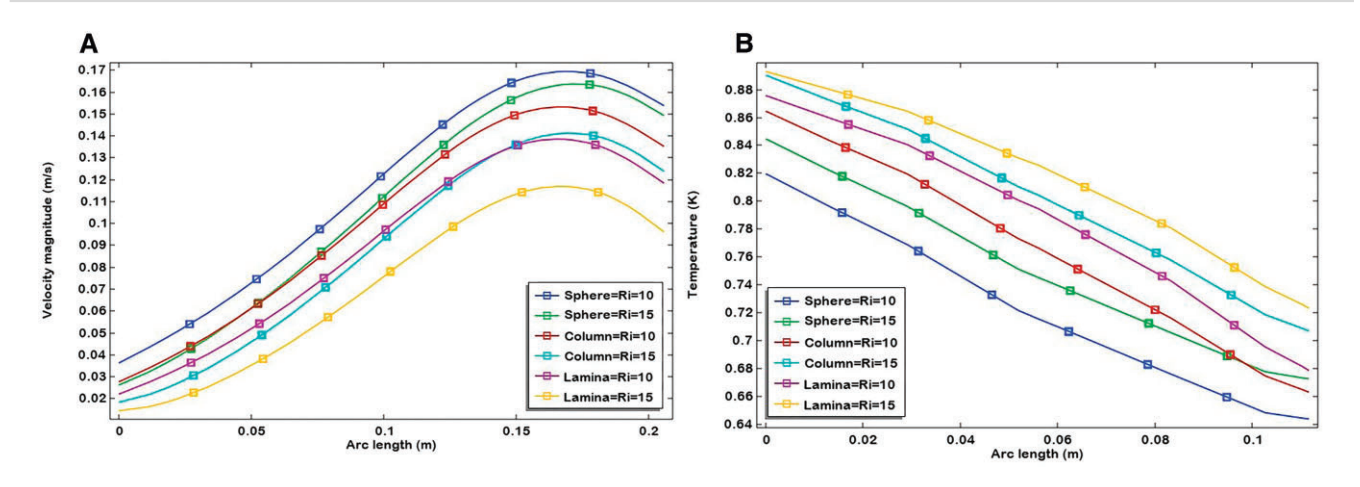


Figure 7: Influence of Ri: (A) on the velocity profile and (B) temperature distribution against different nanoparticle shapes (sphere, column, lamina).

(13)

Table 5: Impact of Ri on K.E.

Shapes	Ri	Kinetic energy
Sphere	10	0.0 064 341
_	15	0.0 068 877
Column	10	0.0 078 812
	15	0.0 089 603
Lamina	10	0.0 092 762
	15	0.011 444

Table 6: Impact of Ri on Nu.

Shapes	Ri	Nusselt number
Sphere	10	1.1181
-	15	1.0782
Column	10	1.8686
	15	1.7547
Lamina	10	4.5295
	15	4.2617

## 3. Methodology

To remove the pressure term from Equations 2 and 3, replace the pressure terms from Equations 2 and 3 with a pseudo-constitutive relation  $P = \gamma \left( \frac{\partial U}{\partial X} + \frac{\partial V}{\partial Y} \right)$ . The weak form of Equations 2–4 is

$$\int_{A} \left( U \frac{\partial U}{\partial X} + V \frac{\partial U}{\partial Y} \right) w_{1} dA + \int_{A} \gamma \frac{\partial}{\partial X} \left( \frac{\partial U}{\partial X} + \frac{\partial V}{\partial Y} \right) w_{1} d\Omega 
+ \frac{\nu_{hnf}}{\nu_{f}} \frac{1}{Re} \int_{A} \left( \frac{\partial^{2} U}{\partial X^{2}} + \frac{\partial^{2} U}{\partial Y^{2}} \right) w_{1} d\Omega = 0,$$

$$\int_{A} \left( U \frac{\partial V}{\partial X} + V \frac{\partial V}{\partial Y} \right) w_{2} d\Omega + \int_{A} \gamma \frac{\partial}{\partial y} \left( \frac{\partial U}{\partial X} + \frac{\partial V}{\partial Y} \right) w_{2} d\Omega 
+ \frac{\nu_{hnf}}{\nu_{f}} \frac{1}{Re} \int_{A} \left( \frac{\partial^{2} V}{\partial X^{2}} + \frac{\partial^{2} V}{\partial Y^{2}} \right) w_{2} d\Omega + \frac{(\rho \beta)_{hnf}}{(\rho \beta)_{f}} \Pr \int_{A} \theta d\Omega = 0,$$
(12)

$$\int\limits_{\Omega} \left( U \frac{\partial \theta}{\partial X} + V \frac{\partial \theta}{\partial Y} \right) w_3 d\Omega - \frac{\alpha_{hnf}}{\alpha_f} \frac{1}{PrRe} \int\limits_{\Omega} \left( \frac{\partial^2 \theta}{\partial X^2} + \frac{\partial^2 \theta}{\partial Y^2} \right) w_3 d\Omega = 0.$$

Within the triangular element, the velocity (U, V) and temperature  $(\theta)$  of the current model can be approximated by applying the shape function of the discretized domain  $\{\phi_i\}_{i=1}^n$ . Consider each six-node biquadratic triangular element over the whole domain fellows as

$$U \approx \sum_{j=1}^{N} u_{j} \phi_{j}(X, Y), V \approx \sum_{j=1}^{N} v_{j} \phi_{j}(X, Y), \theta \approx \sum_{j=1}^{N} \theta_{j} \phi_{j}(X, Y). \quad (14)$$

### 4. Results Assessment and Discussion

The present section presents the analysis of the performance of parameters involved in the fluid flow field. Figure 2 is portrayed to illustrate the Phi effects on Streamlines distribution of hybrid nanofluid. It is observed from Figure 2 that increasing the numerical value of Phi the size of Streamlines vortices gets enhanced. Also, it is observed that the Streamlines distribution is more dominant for lamina-shaped than spherical and columnshaped nanoparticles. Figure 3 illustrates the influence of cap Phi on isothermal contours. It is observed from Figure 3 that Isothermal contours below and upper parts of the elliptic obstacle are more pronounced. Since thermal conductivity is directly associated with nanoparticles concentration, as the values of Phi increase the thermal distribution gets stronger in the regime, resulting in an enhanced temperature profile. Also, among other particles shapes the Isothermal distribution is more pronounced for lamina-shape nanoparticles. Figures 4A and B are presented to report the velocity and temperature of the (Cu and Al<sub>2</sub>O<sub>3</sub>)/H<sub>2</sub>O hybrid nanofluid against Phi. The results depict that the velocity of (Cu and Al<sub>2</sub>O<sub>3</sub>)/H<sub>2</sub>O hybrid nanofluid is decreasing (Figure 4A) while the temperature is increasing as a function of Phi (Figure 4B). Physically, as the volume fraction Phi of (Cu and Al<sub>2</sub>O<sub>3</sub>)/H<sub>2</sub>O hybrid nanofluid increases, the fluid's viscosity rises due to the presence of nanoparticles. This higher viscosity hinders the flow, leading to a decrease in velocity. Moreover, Phi is directly related to the thermal conductivity of (Cu and Al<sub>2</sub>O<sub>3</sub>)/H<sub>2</sub>O hybrid nanofluid, leading to an increased heat transfer rate between solid particles. Consequently, this enhances the temperature of the (Cu and Al<sub>2</sub>O<sub>3</sub>)/H<sub>2</sub>O hybrid nanofluid. In the results for the sphere-shaped nanoparticles, the hybrid nanofluid exhibits the highest velocity compared to column- and lamina-shaped nanoparticles. In contrast, lamina-shaped nanoparticles result in the highest temperature. KE and heat transfer rate of hybrid nanofluid with the variation of phi are expressed in Tables 3 and 4. Here, it can be observed

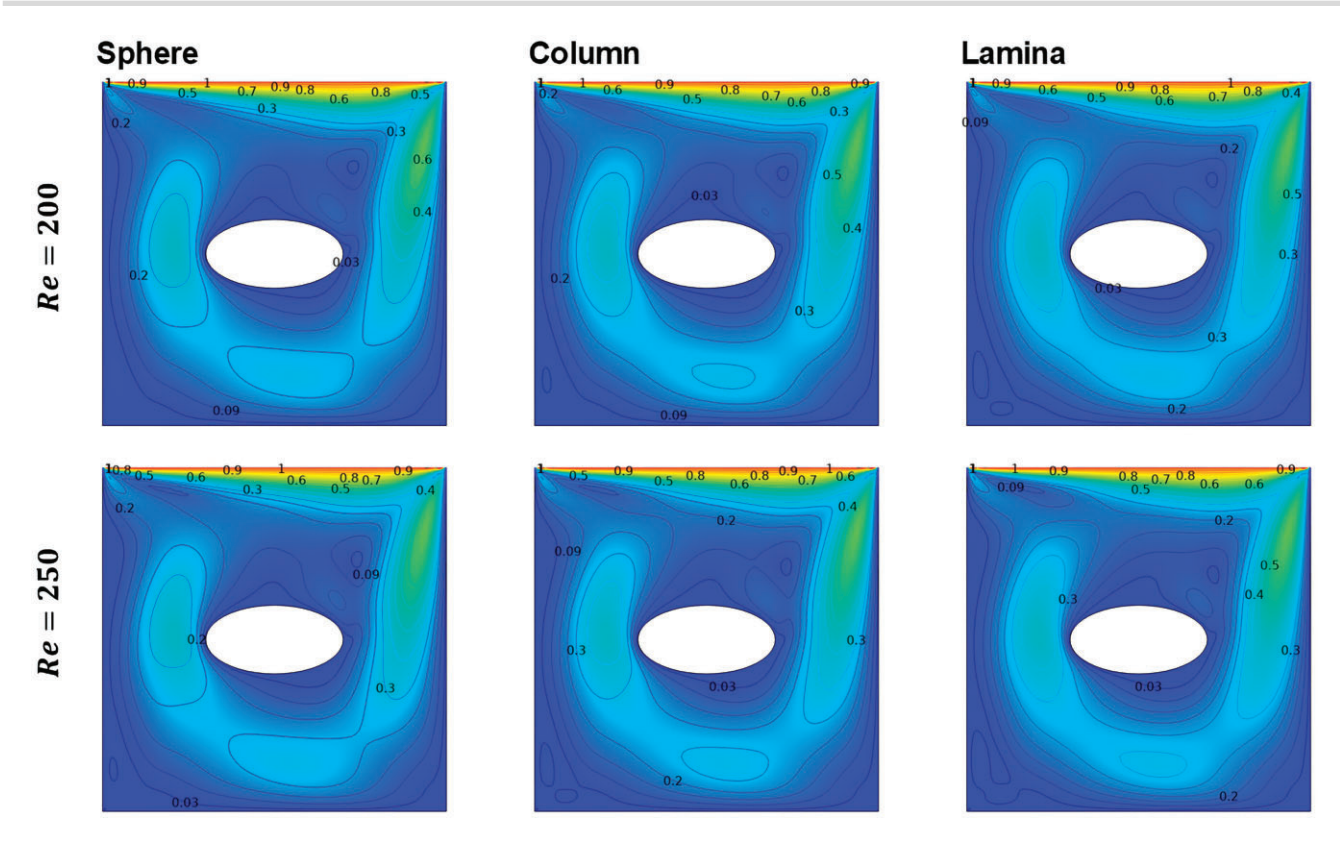


Figure 8: Impact of Re on Streamlines for different nanoparticle shapes (sphere, column, lamina).

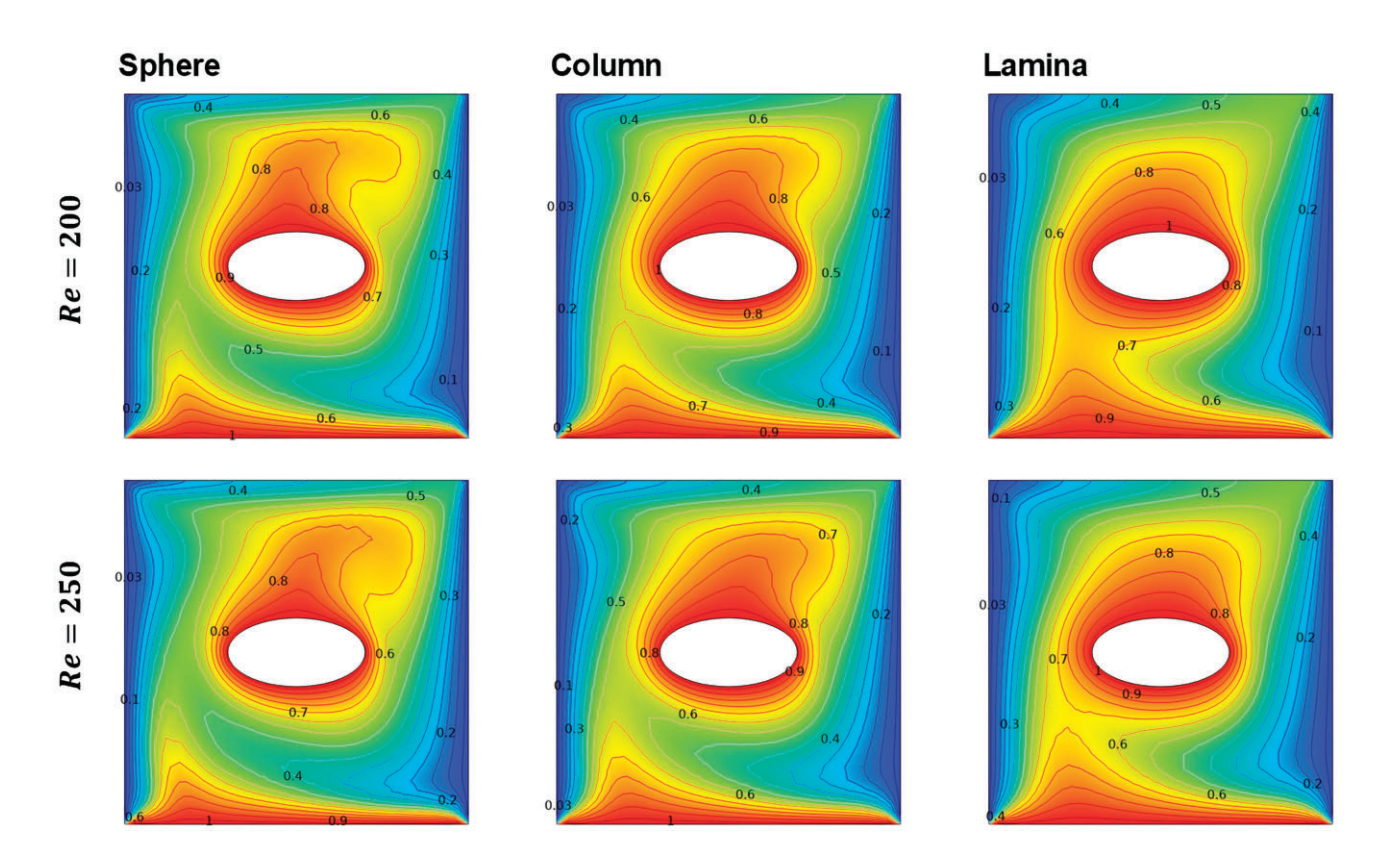


Figure 9: Impact of Re on isotherms for different nanoparticle shapes (sphere, column, lamina).

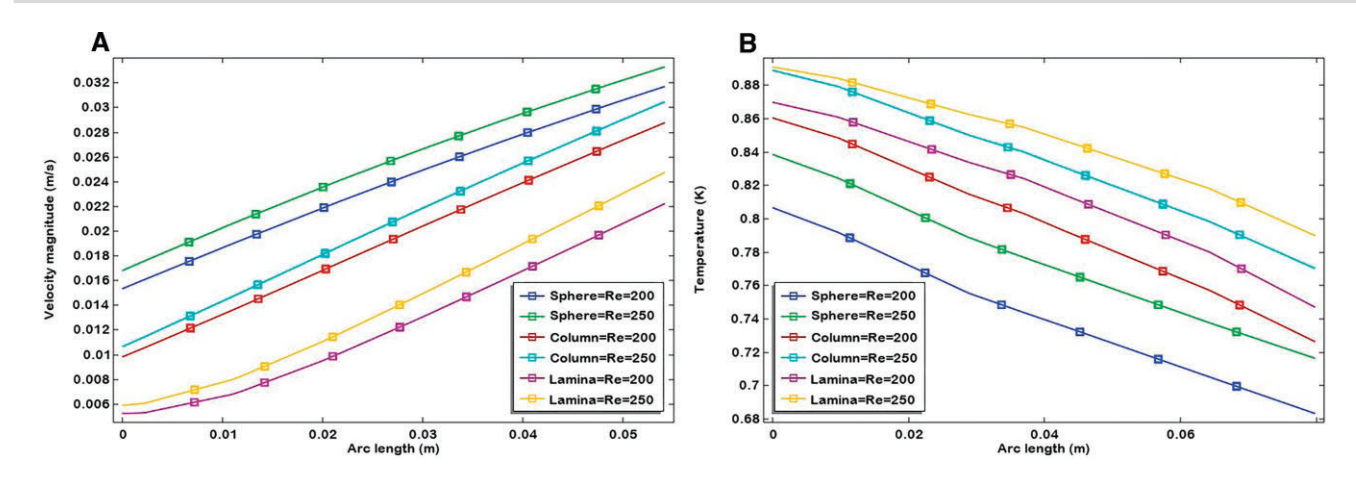


Figure 10: Influence of Re: (A) on the velocity profile and (B) temperature distribution against different nanoparticle shapes (sphere, column, lamina).

Table 7: Impact of Re on KE.

Shape	Re	Kinetic energy
Sphere	200	0.0 020 741
	250	0.0 016 789
Column	200	0.0 019 154
	250	0.0 016 021
Lamina	200	0.0 017 544
	250	0.0 015 210

Table 8: Impact of Re on Nu.

Re	Nusselt number
200	1.1181
250	1.0553
200	1.8686
250	1.7383
200	4.5294
250	4.1103
	200 250 200 250 200

Table 9: Grid independence test.

Grid	EL	DOFs	KE	Error
L1	2394	2451	0.0 025 928	_
L2	3684	3761	0.0 027 383	0.0 001 455
L3	5554	5651	0.0 027 836	0.0 000 453
L4	9214	9351	0.0028524	0.0 000 688
L5	12 238	12 403	0.0028748	0.0 000 224
L6	17 566	17 767	0.0028936	0.0 000 188
L7	43 282	43 675	0.0 029 307	0.0 000 371
L8	113 002	113 755	0.0029428	0.0 000 121
L9	146 292	147 045	0.0 029 435	0.0 000 007

that KE and heat transfer rate possess higher values for sphere and lamina-shaped nano-sized particles, respectively.

Figure 5 illustrates the streamlines for different values of Ri and various nanoparticle shapes. It is observed that as Ri increases, the streamlined distribution strengthens within the enclosure. Additionally, the distribution of Streamlines is more pronounced in the presence of lamina-shaped nanoparticles. For both column and lamina-shaped nanoparticles, the strength of the streamline cells increases as Ri rises. Figure 6 demonstrates the effects of Ri on the Isothermal contours of the hybrid nanofluid. It is reported in Figure 6 that below the elliptic obstacle, the Isothermal contours indicate a reduction in heat intensity as Ri increases. Moreover, compared to other nanoparticle shapes, lamina-shaped nanoparticles result in a higher thermal profile within the Isothermal contours. The impact of Ri on the velocity and temperature of the hybrid nanofluid for various nanoparticle shapes is illustrated in Figures 7A and B. It is observed that as Ri increases, the velocity of the hybrid nanofluid decreases (Figure 7A), while its temperature rises (Figure 7B). Physically, a higher Ri indicates a greater dominance of buoyancy forces over inertial forces. This enhanced buoyancydriven convection strengthens heat transfer, resulting in an overall increase in the temperature of the (Cu and Al<sub>2</sub>O<sub>3</sub>)/H<sub>2</sub>O hybrid nanofluid within the cavity. Tables 5 and 6 show the KE and heat transfer rate with the impact of Ri. It is reported that KE has a direct relation, whereas the heat transfer rate has an inverse relation with Ri. It is observed that the KE and heat transfer rate are maximum in the presence of lamina-shaped nano-sized particles.

Figure 8 depicts the streamlined patterns illustrating the impact of Re for distinct nanoparticle shapes. The results in Figure 8 show that as Re increases, the streamline vortices become more dominant on the right side of the cavity. For sphere, column, and lamina-shaped nanoparticles, the strength of the streamlined cells increases with higher Re, and the size of the streamlined cells also expands for all nanoparticle shapes. The influence of Re on the Isothermal contours is shown in Figure 9. As Re increases, the heat intensity decreases in the regions above and below the elliptic obstacle. Furthermore, the isothermal contours are more dominant in the presence of lamina-shaped nanoparticles compared to other shapes. The variations in velocity and temperature of the hybrid nanofluid under the influence of Re are presented in Figures 10A and B. Figure 10A shows that as Re enhances, the velocity of the hybrid nanofluid rises due to the higher ratio of inertial to viscous forces. Similarly, Figure 10B illustrates that the temperature of the hybrid nanofluid increases with Re, primarily due to the thickening of the thermal boundary layer. Tables 7 and 8 represent the numerical values of the behaviour of KE and rate of heat transfer against Re for various nanoparticle shapes.

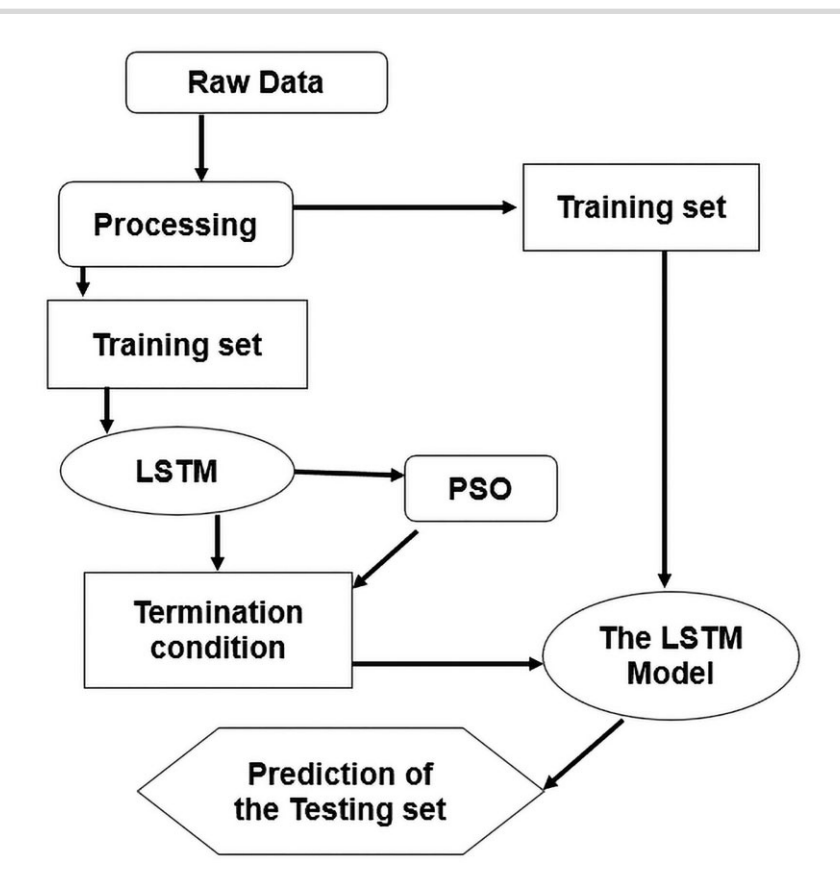


Figure 11: LSTM diagram.

It is noticed from Tables 7 and 8 that the KE and rate of heat transfer are inverse functions of Re. Also, the KE is maximum for sphere-shaped nanoparticles, while the temperature is maximum for lamina-shaped nanoparticles.

### 5. Grid Convergence

To ensure the efficiency of the numerical scheme, multiple grides are displayed in Table 9. Resultantly, the total number of degrees of freedom (DOFs) varies from 2451 to 147045. The difference between KE in the Case of L8 and L9 gride is almost negligible.

### 6. Long Short-Term Memory

LSTM neural network is a form of RNN developed to capture timedependent relationships. LSTM networks possess a specialized cell structure equipped with input, forget, and output gates. To validate the results of the current study, LSTM is used for comparison with the Galerkin Method results. Figure 11 indicates the procedure of LSTM. Figure 12 presents the temperature distribution, comparing numerical results with LSTM predictions and error analysis. The comparison demonstrates excellent accuracy across all nanoparticle shapes, including sphere, column, and lamina. The values of mean absolute error (MAE), mean square error (MSE), root mean square error (RMSE), and coefficient of determination (R2) for each shape of nanoparticles are displayed in Table 10. The table values MAE = 0.04114, MSE = 0.00305, RMSE = 0.0552, and  $R^2 = 0.9676$  for sphere-shaped nanoparticles; MAE = 0.03089, MSE = 0.00184, RMSE = 0.0429, and  $R^2$  = 0.96168 for column-shaped nanoparticles; and MAE = 0.02973, MSE = 0.00185, RMSE = 0.0430, and  $R^2 = 0.962970$  for laminashaped particles, representing the performance of LSTM. The smallest value structure is equipped with MAE, MSE, and RMSE, and the greater value of R2 indicates better performance of the

### 7. Concluding Remarks

A comparative observation of (Cu-Al2O3)/H2O hybrid nanofluid flow inside the lid-driven cavity is presented. The impacts of nanoparticle shapes are also taken into account. The Galerkin Method is applied to solve the mathematical model. To ensure the accuracy of our solution and compare our results, we validated our data using LSTM. The main findings of the current analysis are summarized as

- The lamina (nonspherical) shape nanoparticles (Cu and Al<sub>2</sub>O<sub>3</sub>) in (Cu and Al<sub>2</sub>O<sub>3</sub>)/H<sub>2</sub>O hybrid nanofluid enact an excellent role in the distribution of temperature and heat transfer.
- The sphere (spherical) nanoparticles (Cu and Al<sub>2</sub>O<sub>3</sub>) in (Cu and Al<sub>2</sub>O<sub>3</sub>)/H<sub>2</sub>O hybrid nanofluid present a minor role in temperature distribution and heat transfer.
- The column (nonspherical) shape nano-sized particles (Cu and Al<sub>2</sub>O<sub>3</sub>) in (Cu and Al<sub>2</sub>O<sub>3</sub>)/H<sub>2</sub>O hybrid nanofluid enact an intermediate temperature distribution and heat transfer.

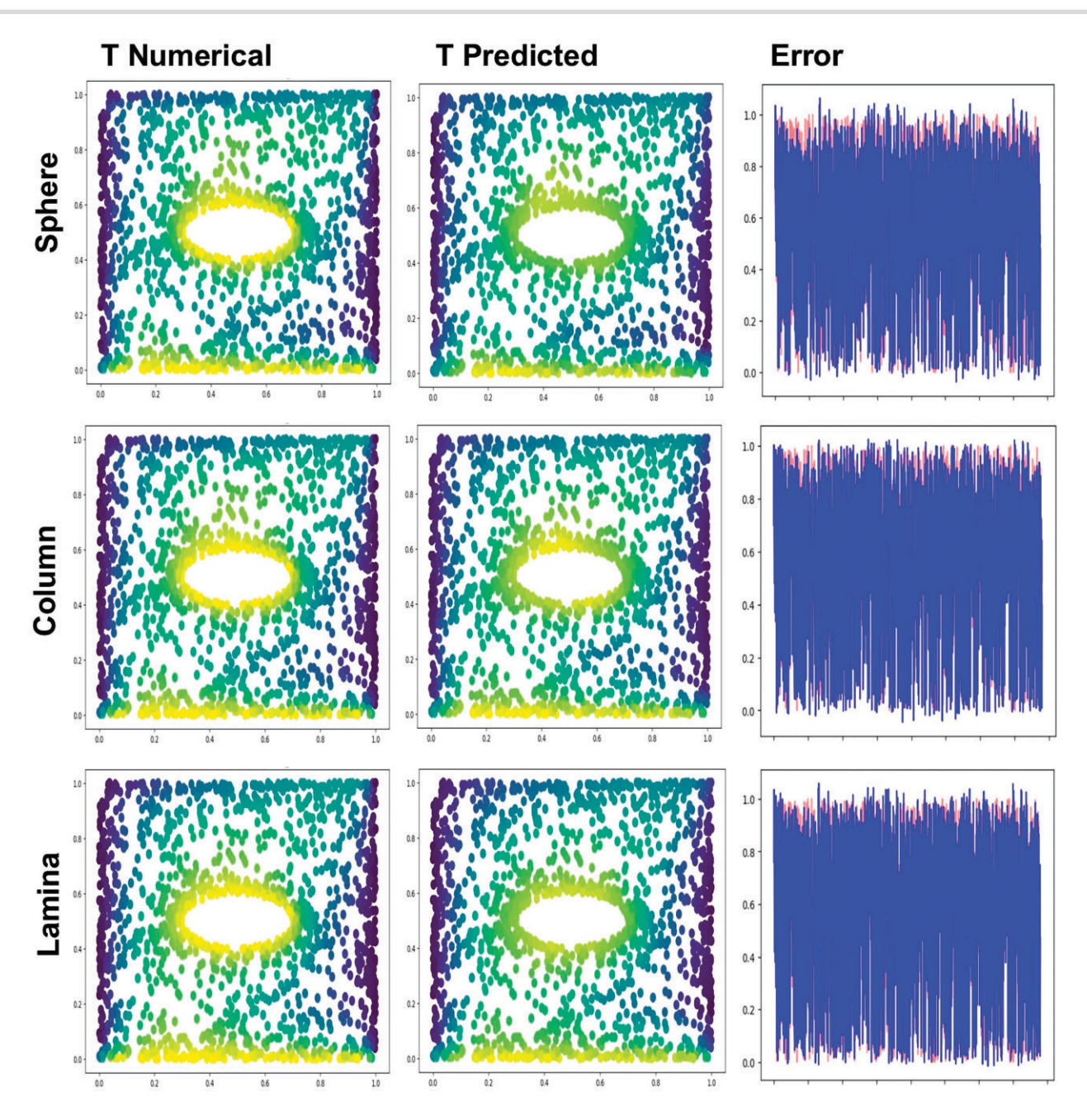


Figure 12: Temperature distribution comparison: the numerical results, LSTM predictions, and error analysis.

Table 10: Values of MAE, MSE, RMSE, and R<sup>2</sup>.

Shapes of nanoparticles	MAE	MSE	RMSE	$\mathbb{R}^2$
Sphere	0.04 114	0.00 305	0.0552	0.9676
Column	0.03 089	0.00 184	0.0429	0.9616
Lamina	0.02 973	0.00 185	0.0430	0.9629

#### **Conflicts of Interest**

The author declares no conflict of interest.

#### **Author Contributions**

Umair Rashid: Conceptualization, Methodology. Ashmore Mawire: Writing review and editing. Kun Yang: Writing—original draft preparation. Ali J. Chamkha: Validation, Investigation, Software. Qingyuan Wang: Supervision.

#### References

Afrand, M., Toghraie, D., & Ruhani, B. (2016). Effects of temperature and nanoparticles concentration on rheological behavior of Fe3O4-Ag/EG hybrid nanofluid: An experimental study. Experimental Thermal and Fluid Science, 77, 38-44. https://doi.org/10.101 6/j.expthermflusci.2016.04.007.

- Ahmad, H., Al-Khaled, K., Sowayan, A. S., Abdullah, M., Hussain, M., Hammad, A., Khan, S. U., & Tlili, I. (2023). Experimental investigation for automotive radiator heat transfer performance with ZnO-Al2O3/water-based hybrid nanoparticles: An improved thermal model. International Journal of Modern Physics B, 37, 2350050. https://doi.org/10.1142/S0217979223500509.
- Akbar, N. S., Zamir, T., Akram, J., Noor, T., & Muhammad, T. (2024). Simulation of hybrid boiling nanofluid flow with convective boundary conditions through a porous stretching sheet through Levenberg Marquardt artificial neural networks approach. International Journal of Heat and Mass Transfer, 228, 125615. https://doi. org/10.1016/j.ijheatmasstransfer.2024.125615.
- Ali, L., Ali, B., Asogwa, K. K., & Apsari, R. (2024). The transient rotating three-dimensional flow of micropolar fluid induced by Riga plate: Finite element approach. Numerical Heat Transfer, Part A: Applications, 85, 1889-1902. https://doi.org/10.1080/10407782.2023.2212
- Al-mdallal, O. M., Indumathi, N., Ganga, B., & Hakeem, A. K. A. (2020). Marangoni radiative effects of hybrid-nanofluids flow past a permeable surface with an greaterinclined magnetic field. Case Studies in Thermal Engineering, 17, 100571. https://doi.org/10.1016/j.cs ite.2019.100571.
- Aziz, A., Jamshed, W., & Aziz, T. (2018). Mathematical model for thermal and entropy analysis of thermal solar collectors using Maxwell nanofluids with slip conditions, thermal radiation and variable thermal conductivity. Open Physics, 16, 123-136. https: //doi.org/10.1515/phys-2018-0020.
- Babazadeh, H., Shah, Z., Ullah, I., Kumam, P., & Shafee, A. (2020). Analysis of hybrid nanofluid behavior within a porous cavity, including Lorentz forces and radiation impacts. Journal of Thermal Analysis and Calorimetry, 143, 1129-1137. https://doi.org/10.1007/s10973-0 20-09416-1.
- Beaufays, F., Sak, H., & Senior, A. (2014). Long short-term memory recurrent neural network architectures for large scale acoustic modeling has. Interspeech, September, 338-342.
- Bhuiyana, A., Alam, M. S., & Alim, M. (2017). Natural convection of water-based nanofluids in a square cavity with partially heated of the bottom wall. Procedia Engineering, 194, 435–441. https://doi. org/10.1016/j.proeng.2017.08.168.
- Caldorera-Moore, M., Guimard, N., Shi, L., & Roy, K. (2010). Designer nanoparticles: Incorporating size, shape and triggered release into nanoscale drug carriers. Expert Opinion on Drug Delivery, 7, 479-495. https://doi.org/10.1517/17425240903579971.
- Chang, S., Dong, W., & Jun, H. (2020). Use of electroencephalogram and long short-term memory networks to recognize design preferences of users toward architectural design alternatives. Journal of Computational Design and Engineering, 7, 551-562. https://doi.or g/10.1093/jcde/qwaa045.
- Fayz-Al-Asad, M., Iqbal, Z., Hasan, M. S., Eljaneid, N. H., Alam Sarker, M. M., Alhazmi, S. E., Shah, J., Alqarni, M., Awwad, T. M., & Elnageeb, T. (2024). Computational modelling and simulations to study the thermal enhancement in nanofluid flow in a undulating wavy cavity of a cylinder: Finite element analysis. Journal of Computational Design and Engineering, 12, 130-144.
- Hochreiter, S. (1997). Long Short-term Memory. Neural Computation
- Hughes, T. J., Liu, W. K., & Brooks, A. (1979). Finite element analysis of incompressible viscous flows by the penalty function formulation. Journal of Computational Physics, 30, 1-60. https://doi.org/10.1 016/0021-9991(79)90086-X.
- Ibrahim, W., & Lamesse, T. (2023). Powell-eyring nanofluid analysis with finite element method when past a stretching sheet with convective heating and passive control of nanoparticle. Interna-

- tional Journal of Thermofluids, 19, 100388. https://doi.org/10.1016/j. ijft.2023.100388.
- Jamil, F., & Ali, H. M. (2020). Applications of hybrid nanofluids in different fields. In Hybrid Nanofluids for Convection Heat Transfer. (pp. 215-254). Elsevier.
- Khan, A., Saeed, A., Tassaddiq, A., Gul, T., Majmaah, I. S., & Technology, I. (2011). Bio-convective and chemically reactive hybrid nanofluid flow upon a thin stirring needle with viscous dissipation. Scientific Reports, 11, 1-29. https://doi.org/10.1038/s41598-0 21-86968-8.
- Knauer, A., & Koehler, J. M. (2016). Explanation of the size-dependent in-plane optical resonance of triangular silver nanoprisms. Physical Chemistry Chemical Physics, 18, 15943–15949. https://doi.org/10 .1039/c6cp00953k.
- Madhu, M., & Kishan, N. (2015). Finite element analysis of MHD viscoelastic nanofluid flow over a stretching sheet with radiation. Procedia Engineering, 127, 432-439. https://doi.org/10.1016/j.proe
- Khashi'ie, N. S., Arifin, N. M., Pop, I., Nazar, R., Hafidzuddin, M. E. H., & Wahi, N. (2020). Thermal marangoni flow past a permeable stretching /shrinking sheet in a hybrid. Sains Malaysiana, 49, 211-222. https://doi.org/10.17576/jsm-2020-4901-25.
- Nithiarasu, P., & Zienkiewicz, O. Z. (2006). The finite element method for heat and fluid flow. International Heat Transfer Conference 13.
- Qian, F., Chen, L., Li, J., Ding, C., Chen, X., & Wang, J. (2019). Direct prediction of the toxic gas diffusion rule in a real environment based on LSTM. International Journal of Environmental Research and Public Health, 16, 2133. https://doi.org/10.3390/ijerph16122133.
- Qureshi, M. Z. A., Raza, Q., Eldin, S. M., Zafar, M., Ali, B., & Siddique, I. (2023). Thermal performance of hybrid magnetized nanofluids flows subject to joint impact of ferro oxides/CNT nanomaterials with radiative and porous factors. Case Studies in Thermal Engineering, 41, 102648. https://doi.org/10.1016/j.csite.2022.102648.
- Rashid, U., Akgül, A., & Lu, D. (2023a). Impact of nanosized particles on hybrid nanofluid flow in porous medium with thermal slip condition. Numerical Heat Transfer, Part B: Fundamentals, (pp. 1-14). Taylor & Francis Inc.
- Rashid, U., & Ibrahim, A. (2020). Impacts of nanoparticle shape on Al2O3-water nanofluid flow and heat transfer over a non-linear radically stretching sheet. Advances in Nanoparticles, 09, 23-39. ht tps://doi.org/10.4236/anp.2020.91002.
- Rashid, U., Lu, D., & Iqbal, Q. (2023b). Nanoparticles impacts on natural convection nanofluid flow and heat transfer inside a square cavity with fixed a circular obstacle. Case Studies in Thermal Engineering, 102829.
- Sakkaravarthi, K., Reddy, P. B. A., & Sakthi, I. (2024). Entropy optimization in Casson tetra-hybrid nanofluid flow over a rotating disk with nonlinear thermal radiation: A Levenberg-Marquardt neural network approach. Journal of Computational Design and Engineering, 11, 333-354. https://doi.org/10.1093/jcde/qwae086.
- Selvaggio, A. Z., Sousa, F. M. M., da Silva, F. V., & Vianna, S. S. (2022). Application of long short-term memory recurrent neural networks for localisation of leak source using 3D computational fluid dynamics. Process Safety and Environmental Protection, 159, 757-767. https://doi.org/10.1016/j.psep.2022.01.021.
- Sohail, M., Nazir, U., Singh, A., Tulu, A., & Khan, M. J. (2024). Finite element analysis of cross fluid model over a vertical disk suspended to a tetra hybrid nanoparticles mixture. Scientific Reports, 14, 1520. https://doi.org/10.1038/s41598-024-51262-w.
- Srinivasa, R. R., Jithender, G., Anand, J., & Rashidi, M. (2016). Thermal diffusion and diffusion thermo effects on an unsteady heat and

- mass transfer magnetohydrodynamic natural convection couette flow using FEM. *Journal of Computational Design and Engineering*, **3**, 349–362.
- Truong, N. P., Whittaker, M. R., Mak, C. W., & Davis, T. P. (2017). Ortance of nanoparticle shape in cancer drug delivery the importance of nanoparticle shape in cancer drug delivery. Expert Opinion on Drug Delivery, 12, 129–142. https://doi.org/10.1517/17425247.2014.9505
- Waini, I., Ishak, A., & Pop, I. (2020). Hybrid nanofluid flow towards a stagnation point on a stretching/shrinking cylinder. *Scientific Reports*, **10**, 1–12. https://doi.org/10.1038/s41598-020-66126-2.
- Zhang, Q., Yang, L. T., Chen, Z., & Li, P. (2018). A survey on deep learning for big data. *Information Fusion*, **42**, 146–157. https://doi.org/10.1016/j.inffus.2017.10.006.
- Zhao, Y., Wang, Y., Ran, F., Cui, Y., Liu, C., Zhao, Q., Gao, Y., Wang, D., & Wang, S. (2017). A comparison between sphere and rod nanoparticles regarding their in vivo biological behaviour and pharmacokinetics. Scientific Reports, 7, 1–11. https://doi.org/10.1038/s41598-017-03834-2.
- Zhu, X., Vo, C., Taylor, M., & Smith, B. R. (2019). Non-spherical microand nanoparticles in nanomedicine. *Materials Horizons*, **6**, 1094– 1121. https://doi.org/10.1039/c8mh01527a.